ENSTA Bretagne · Ifremer
15ÈMES JOURNÉES DE L'HYDRODYNAMIQUE
22 - 24 novembre 2016 - Brest

DEVELOPMENT OF A HYBRID LBM-POTENTIAL FLOW MODEL FOR NAVAL HYDRODYNAMICS

DEVELOPPEMENT D'UN MODÈLE HYBRIDE LBM-POTENTIEL POUR L'HYDRODYNAMIQUE NAVALE

C.M. O'REILLY[1,2], S.T. GRILLI[1], J.C. HARRIS[3], A. MIVEHCHI[1], C.F. JANSSEN[4], J.M. DAHL[1]

[1] Dept. of Ocean Engineering, University of Rhode Island, Narragansett, RI 02882, USA
[2] Navatek Ltd., South Kingstown, RI 02879, USA
[3] LHSV, Ecole des Ponts, CEREMA, EDF R&D, Université Paris-Est, Chatou, France
[4] Fluid Dynamics and Ship Theory Inst., Hamburg University of Technology (TUHH), Germany
coreilly@navatekltd.com

Summary

We report on the validation of a 3D hybrid model for naval hydrodynamics based on a perturbation method, where velocity and pressure are the sum of an inviscid flow with a viscous perturbation. The far- to near-field inviscid flows can be solved with a BEM, based on potential flow theory and the near-field perturbation flow is solved with a NS model based on a Lattice Boltzmann Method (LBM). We give the model formulation and latest developments in LES turbulence modeling, including a wall model. We validate these by simulating flows over a flat plate for $\mathrm{Re} \in [3.7 \times 10^4; 1.2 \times 10^6]$, for which the plate friction coefficient agrees well with experiments. We also simulate the flow past a foil for $\mathrm{Re} = 3 \times 10^6$ and show good agreement of lift forces with experiments. Results obtained with the hybrid model are nearly identical to those of the LBM alone, but with a smaller computational domain, demonstrating the benefits of this approach.

Résumé

Nous présentons un modèle hybride pour l'hydrodynamique navale, basé sur une méthode de perturbation décomposant la vitesse et la pression en la somme d'un écoulement non-visqueux et d'une perturbation visqueuse. Les équations des champs lointain à proche sont résolues par une méthode potentielle BEM et celles des écoulements en champ proche par un modèle NS basé sur la méthode "Lattice Boltzmann" (LBM). Nous résumons la formulation du modèle et ses derniers développements en modélisation LES de la turbulence avec un "wall model" (couche limite visqueuse-turbulente). Ceux-ci sont validés pour l'écoulements au dessus d'une plaque pour $\mathrm{Re} \in [3.7 \times 10^4; 1.2 \times 10^6]$; le coefficient de frottement sur la plaque est en bon accord avec l'expérience. Nous simulons l'écoulement autour d'un hydrofoil pour $\mathrm{Re} = 3 \times 10^6$ et montrons un bon accord avec l'expérience. Les résultats obtenus avec le modèle hybride sont très proches de ceux du modèle LBM seul, mais pour un domaine de calcul plus petit, ce qui montre l'avantage de cette approche.

I – Introduction

The simulation of large ship motions and resistance in steep waves is typically performed using linear or nonlinear potential flow solvers, usually based on a higher-order Boundary Element Method (BEM), with semi-empirical corrections introduced to account for viscous/turbulent effects. However in some cases, viscous/turbulent flows near the ship's hull and breaking waves and wakes must be accurately modeled to capture the salient physics. Navier-Stokes (NS) solvers can and have been used to model such flows, but they are computationally expensive and often too numerically dissipative to model wave propagation over long distances.

Here, we detail the development of a 3D hybrid model, for solving naval hydrodynamics problems, based on a perturbation method (e.g., Alessandrini, 2007 ; Grilli, 2008 ; Harris and Grilli, 2012), in which both velocity and pressure are expressed as the sum of an inviscid (I) and a viscous perturbation (P) component. In this model, the far- to near-field inviscid flow is solved with a BEM, based on fully nonlinear potential flow (FNPF) theory, also referred to as Numerical Wave Tank (NWT), and the near-field perturbation flow is solved with a NS model, here implemented with a Lattice Boltzmann Method (LBM ; e.g., d'Humieres et al., 2002 ; Janssen, 2010 ; Janssen et al., 2010) including a Large Eddy Simulation of the turbulence (LES ; e.g., Krafczyk et al., 2003). Both the BEM and LBM models have separate representations of the free surface (using an explicit Eulerian-Lagrangian time updating in the former and a VOF method in the latter ; e.g., O'Reilly et al., 2015).

In the context of the hybrid perturbation method, the LBM is only applied to the near-field where viscous/turbulent effects matter, and its solution is forced by results of the NWT applied to the entire domain. Hence the hybrid approach increases computational efficiency relative to traditional CFD solutions, in which the NS solver is applied to the entire domain. This was already demonstrated by Reliquet et al. (2014) based on different types of models, which were less efficient and optimized than those proposed here. Indeed, the NWT used here was the object of numerous developments over the past two decades (see Grilli et al.'s, 2010 review to date). Its latest version was optimized with a Fast Multipole Method (FMM), based on the parallel ExaFMM library, and shown to achieve nearly linear scaling on large CPU clusters (e.g., Harris et al., 2014 and Harris et al., in this conference). The LBM has proved to be accurate and efficient for simulating a variety of complex fluid flow and fluid-structure interaction problems and, when implemented on a massively parallel General Purpose Graphical Processor Unit (GPGPU) co-processor, it was also shown to achieve very high efficiency (over 100 million node updates per second on a single GPGPU ; e.g., Janssen, 2010 ; Janssen et al., 2013 ; Banari et al., 2014). In this respect, LBM developments in this work are based on the highly efficient, GPGPU-accelerated, Lattice Boltzmann solver ELBE (Janssen et al., 2015 ; www.tuhh.de/elbe), developed at TUHH, which features various LBM models, an on-device grid generator, higher-order boundary conditions, and the possibility of specifying overlapping nested grids. ELBE also includes the initial LBM perturbation model based on Janssen et al.'s (2010) approach (discussed later). Simple validations of the hybrid LBM and LBM-LES approaches, for viscous and turbulent oscillatory boundary layers, were reported by O'Reilly et al. (2015) and Janssen et al. (2016).

In this paper, we focus on the development and validation of the hybrid NS-LBM solver applied to the perturbation flow and, in this context, the modeling of turbulent flows by a LES, and by an accurate representation of boundary layers near solid boundaries without the need for a refined discretization. We first summarize the principles of the LBM, in particular when using the more accurate Multiple Relaxation Time (MRT) method. We then detail the formulation of the perturbation method in the context of turbulent flows and show how the

standard LES equations are modified. The hybrid LBM-LES approach is then validated by solving turbulent flows past a solid boundary and retrieving the "law of the wall". Finally, the method is validated by computing the drag and lift coefficients of a hydrofoil at high Reynolds number.

II – Methodology

II – 1 Lattice Boltzmann Method (LBM)

In the LBM, the macroscopic NS equations are modeled by solving an equivalent mesoscopic problem in which the fluid is represented by particles interacting over a (typically regular) lattice (or grid), through their distribution functions (DF) $f(t, \mathbf{x}, \xi)$, representing the normalized probability to find a particle at location $\mathbf{x}$ at time t with velocity ξ ; the macroscopic hydrodynamic quantities (e.g., velocity, pressure,...) are defined as moments of the DFs.

The time evolution of discrete particle DFs is governed by the Boltzmann advection-collision equation,

$$\frac{Df_\alpha}{Dt} = \frac{\partial f_\alpha(t,\mathbf{x})}{\partial t} + \mathbf{e}_\alpha \cdot \frac{\partial f_\alpha(t,\mathbf{x})}{\partial \mathbf{x}} = \Omega_\alpha + B_\alpha \tag{1}$$

in which $\mathbf{e}_\alpha$ denotes discrete particle velocities, Ω_α is a collision operator describing interactions between particles, and B_α represents volume forces such gravity. Eq. (1) is discretized over a regular lattice, of grid spacing Δx using $n = 19$ discrete particle velocities, which point in the directions of 18 neighboring particles from a given particle location ; thus : $\mathbf{e}_\alpha = \{0,0,0\}; \{\pm c,0,0\}; \{0,\pm c,0\}; \{0,0,\pm c\}; \{\pm c,\pm c,0\}; \{\pm c,0,\pm c\}; \{0,\pm c,\pm c\}$, for $\alpha = 0, ..., 18$ (standard D3Q19 scheme). The constant velocity $c = \sqrt{3}c_s$ is related to the speed of sound c_s.

In the standard single relaxation time (SRT) LBM, Eq. (1) is discretized by finite differences in space and time as,

$$f_\alpha(t+\Delta t, \mathbf{x}+\mathbf{e}_\alpha \Delta t) - f_\alpha(t,\mathbf{x}) = -\frac{1}{\tau}\{f_\alpha(\mathbf{x},t) - f_\alpha^{eq}(\rho,\mathbf{u})\} + B'_\alpha \tag{2}$$

where $f_\alpha^{eq}(\rho,\mathbf{u})$ are equilibrium DFs, functions of the macroscopic fluid density ρ and velocity $\mathbf{u}$, Δt is time step (with $c = \Delta x/\Delta t$), and $\tau = 3\nu/c^2 + \Delta t/2$, a nondimensional relaxation time (SRT) expressed as a function of fluid viscosity ν. LBM simulations are typically split up into a local *collision* step, which locally drives the particle DFs to equilibrium, and a *propagation* step, during which the evolved DFs are advected. The hydrodynamic quantities are found as low order moments of the DFs,

$$\rho = \sum_{\alpha=1}^{n} f_\alpha, \qquad \rho\,\mathbf{u} = \sum_{\alpha=1}^{n} \mathbf{e}_\alpha f_\alpha \tag{3}$$

Applying a Chapman-Enskog expansion to Eq. (2) (see, e.g., Banari et al., 2014) yields,

$$f_\alpha^{eq}(\rho,\mathbf{u}) = w_\alpha \left(\rho + \rho_o\left(3\frac{(\mathbf{u}\cdot\mathbf{e}_\alpha)}{c^2} + \frac{9}{2}\frac{(\mathbf{u}\cdot\mathbf{e}_\alpha)^2}{c^4} - \frac{3}{2}\frac{\mathbf{u}^2}{c^2}\right)\right) \tag{4}$$

for the LBM solution to satisfy the incompressible NS equations up to $\mathcal{O}(\Delta x^2)$ and $\mathcal{O}(\mathrm{Ma}^2)$ errors, with Ma the Mach number ; ρ_o and ρ represent the average fluid density and a small perturbation from that density, respectively, and w_α are lattice dependent directional weights with, $w_0 = 1/3$, $w_{1...6} = 1/18$ and $w_{7...18} = 1/36$.

The collision step in Eq. (2) is a strictly local operation between neighboring lattice nodes while the convective step simply propagates the particle distribution functions in their discretized velocity directions $\mathbf{e}_\alpha$. Unlike standard NS solvers used in CFD the LBM solution does not require a pressure correction step as pressure is simply given by $p = c_s^2\rho$. This locality of all LBM numerical operations makes it very well suited to massively parallel computations on a GPGPU.

d'Humieres et al. (2002) showed that more accurate and stable results can be obtained, particularly for high Reynolds numbers Re, using the multiple relaxation time (MRT) LBM. This method incorporates higher-order moments (i.e., hydrodynamic quantities and their fluxes) into the solution, which have important physical significance (Lallemand and Lou 2000) and will be useful to implement the LES in the LBM for turbulent flows (see below). In the MRT, the collision operator in the right hand side of Eq. (2) is replaced by ($\beta = 0, ..., 18; \gamma, \delta = 0, ..., 15$; repeated indices in equations mean an implicit summation),

$$\Omega_\alpha = -M^{-1}_{\alpha\gamma} S_{\gamma\delta}(M_{\beta\delta} f_\beta - m^{eq}_\delta) \tag{5}$$

where $M_{\alpha\gamma}$ is the transformation matrix from DFs to moments, with $f_\alpha = M^{-1}_{\alpha\gamma} m_\gamma$ and $S_{\gamma\delta}$ is a diagonal collision matrix of relaxation parameters, weighing different properties of the fluid (see references). Equilibrium moments m^{eq}_γ are derived from the $f^{eq}_\alpha(\mathbf{x}, t)$ as,

$$\begin{aligned} m^{eq}_0 = \rho, \quad m^{eq}_3 = \rho u_x, \quad m^{eq}_5 = \rho u_y, \quad m^{eq}_7 = \rho u_z \\ m^{eq}_1 = e^{eq} = \rho_0(u_x^2 + u_y^2 + u_z^2), \quad m^{eq}_9 = 3p^{eq}_{xx} = \rho_0(2u_x^2 - u_y^2 - u_z^2) \\ m^{eq}_{11} = p^{eq}_{zz} = \rho_0(u_y^2 - u_z^2), \quad m^{eq}_{13} = p^{eq}_{xy} = \rho_0(u_x u_y) \\ m^{eq}_{14} = p^{eq}_{yz} = \rho_0(u_y u_z), \quad m^{eq}_{15} = p^{eq}_{xz} = \rho_0(u_x u_z) \end{aligned} \tag{6}$$

In the following, prime variables will denote non-dimensional variables where lengths have been divided by a length scale λ, times by time scale τ, and mass by mass scale ϖ ; thus, $c' = c\tau/\lambda = \Delta x'/\Delta t'$. The numerical solution in LBM models is typically stable for a mesh Courant number of 1, yielding, $c' = 1$; one also typical assumes, $\lambda = \Delta x$, thus $\Delta x' = 1 \rightarrow \Delta t' = 1$; finally the nondimensional viscosity reads, $\nu' = \nu\tau/\lambda^2$. In LBM simulations of flows at specified Mach and Reynolds numbers (Ma, Re), one thus finds, $\nu' = c'_s \ell' \mathrm{Ma}/\mathrm{Re}$, to use in simulations, also given the physical length scale of the flow ℓ.

II – 2 Equations for the perturbation LBM

Here, we first recap the expressions of the NS perturbation method (Grilli, 2008 ; Harris and Grilli, 2012) and develop the corresponding LBM equations with MRT. In the NS perturbation approach, both the flow velocity and pressure are expressed as,

$$u_i = u^I_i + u^P_i \qquad \text{with} \qquad \tilde{p} = \tilde{p}^I + \tilde{p}^P \tag{7}$$

where $\tilde{p} = p + \rho g x_3 - \frac{2}{3}\rho k$ denotes the perturbation dynamic pressure, with k the turbulent kinetic energy. Recall that superscripts I denote irrotational flow quantities, with $u^I_i = \nabla_i \phi^I$ satisfying Euler equations, and superscripts P represents perturbation flow quantities that are driven by the inviscid flow fields. After applying this decomposition and substituting Euler's equations, the perturbation NS equations read,

$$\frac{\partial u^P_i}{\partial x_i} = 0 \tag{8}$$

$$\frac{\partial u^P_i}{\partial t} + u^P_j \frac{\partial u^P_i}{\partial x_j} = -\frac{1}{\rho}\frac{\partial \tilde{p}^P}{\partial x_i} + (\nu + \nu_t)\frac{\partial^2 u^P_i}{\partial x_j \partial x_j} - \left(\frac{\partial u^I_i}{\partial x_j} u^P_j + u^I_j \frac{\partial u^P_i}{\partial x_j}\right) + 2\frac{\partial \nu_t}{\partial x_j} S_{ij} \tag{9}$$

where ν and ν_t are kinematic molecular and turbulent viscosity, respectively, with the latter being expressed through the Smagorinsky method as,

$$\nu_t = (C_S\Delta)^2|\mathbf{S}|, \quad \text{with} \quad S_{ij} = S_{ij}^P + S_{ij}^I = \frac{1}{2}\left(\frac{\partial u_i^P}{\partial x_j} + \frac{\partial u_j^P}{\partial x_i} + \frac{\partial u_i^I}{\partial x_j} + \frac{\partial u_j^I}{\partial x_i}\right) \tag{10}$$

where C_S is the Smagorinsky constant, Δ a grid filtering length scale, and S_{ij} the rate of strain tensor is the sum of components functions of the perturbation (S_{ij}^P) and inviscid (S_{ij}^I) velocity.

Janssen et al. (2010) developed a perturbation LBM-LES with MRT solving Eqs. (7) to (10), in which the "I-P" interactions terms were treated as volume forces through the B'_α terms of Eq. (2). Here, instead, we solve these equations, assuming the perturbation LBM-LES DFs are decomposed as, $f_\alpha = f_\alpha^I + f_\alpha^P$ and introduced in Eq. (2). Substracting from the latter the LBM equation for the inviscid flow, we find,

$$f_\alpha^P(t+\Delta t, \mathbf{x}+\mathbf{e}_\alpha\Delta t)) - f_\alpha^P(t,\mathbf{x})) = -\frac{1}{\tau}\{f_\alpha^P(t,\mathbf{x}) - f_\alpha^{eq}(\rho^I+\rho^P, \mathbf{u}^I+\mathbf{u}^P) + f_\alpha^{eq,I}(\rho^I,\mathbf{u}^I)\} \tag{11}$$

where the $f_\alpha^{eq,I}(\rho^I,\mathbf{u}^I)$ are expressed with Eq. (4) based on inviscid fields and satisfy,

$$\sum_{\alpha=1}^{n} f_\alpha^{eq,I} = 0, \quad \sum_{\alpha=1}^{n} e_{\alpha i} f_\alpha^{eq,I} = \rho_o u_i^I, \quad \sum_{\alpha=1}^{n} e_{\alpha i} e_{\alpha j} f_\alpha^{eq,I} = p^I\delta_{ij} + \rho_o u_i^I u_j^I \tag{12}$$

The perturbation equilibrium DFs are then found as, $f_\alpha^{eq,P}(\rho^P,\mathbf{u}^P,\mathbf{u}^I) = f_\alpha^{eq}(\rho^I+\rho^P,\mathbf{u}^I+\mathbf{u}^P) - f_\alpha^{eq,I}(\rho^I,\mathbf{u}^I)$,

$$f_\alpha^{eq,P} = w_\alpha\left(\rho^P + \rho_o\left(3\frac{\mathbf{u}^P\cdot\mathbf{e}_\alpha}{c_s^2} + \frac{9}{2}\frac{(\mathbf{e}_\alpha\cdot\mathbf{u}^P)^2 + 2(\mathbf{e}_\alpha\cdot\mathbf{u}^P)(\mathbf{e}_\alpha\cdot\mathbf{u}^I)}{c_s^4} - \frac{3}{2}\frac{(\mathbf{u}^P)^2}{c_s^2}\right)\right), \tag{13}$$

which satisfy,

$$\sum_{\alpha=1}^{n} f_\alpha^{eq,P} = \rho^P, \quad \sum_{\alpha=1}^{n} e_{\alpha i} f_\alpha^{eq,P} = \rho_o u_i^P, \quad \sum_{\alpha=1}^{n} e_{\alpha i} e_{\alpha j} f_\alpha^{eq,P} = p^P\delta_{ij} + \rho_o u_i^I u_j^P + \rho_o u_i^P u_j^I + \rho_o u_i^P u_j^P \tag{14}$$

A rigorous Chapman-Enskog expansion would show that the perturbation NS Eqs. (7) to (10) are recovered when using these DFs. Note the interaction terms between the I and P fields in Eqs. (13) and (14) expressing the inviscid flow forcing on the perturbation fields.

Extending this formulation to the MRT, assuming a collision operator expressed by Eq. (5), we find the equilibrium moments,

$$\begin{aligned}
m_1^{eq} = e^{eq} &= \rho_0((u_x^P)^2 + (u_y^P)^2 + (u_z^P)^2 + 2u_x^P u_x^I + 2u_y^P u_y^I + 2u_z^P u_z^I) \\
m_9^{eq} = 3p_{xx}^{eq} &= \rho_0(2(u_x^P)^2 - (u_y^P)^2 - (u_z^P)^2 + 4u_x^P u_x^I - 2u_y^P u_y^I - 2u_z^P u_z^I) \\
m_{11}^{eq} = p_{zz}^{eq} = \rho_0((u_y^P)^2 - (u_z^P)^2 + 2u_y^P u_y^I - 2u_z^P u_z^I), &\quad m_{13}^{eq} = p_{xy}^{eq} = \rho_0(u_x^P u_y^P + u_x^P u_y^I + u_y^P u_x^I) \\
m_{14}^{eq} = p_{yz}^{eq} = \rho_0(u_y^P u_z^P + u_y^P u_z^I + u_z^P u_y^I), &\quad m_{15}^{eq} = p_{xz}^{eq} = \rho_0(u_x^P u_z^P + u_x^P u_z^I + u_z^P u_x^I)
\end{aligned} \tag{15}$$

Moments that are not listed above are unchanged from the standard MRT formulation.

II – 3 LES turbulence modeling with a LBM

Krafczyk et al. (2003) expressed the 2nd-order moments of the DFs as,

$$P_{ij} = \sum_{\alpha=1}^{n} e_{\alpha i} e_{\alpha j} f_\alpha = c_s^2 \rho_o \delta_{ij} + \rho_o u_i u_j - \frac{2c_s^2\,\rho}{s_2}\, S_{ij} \tag{16}$$

where s_2 is a relaxation rate for these moments, and showed that they are related to 2nd-order moments in the MRT, $3p_{xx}$, p_{zz}, p_{xy}, p_{yz}, and p_{xz}. The 1st and 2nd terms in Eq. (16)'s RHS are functions of flow quantities obtained through other moments of the DFs. Based on Eq. (16), the rate of strain tensor can be expressed as,

$$S_{ij} = \frac{s_2}{2c_s^2\rho}\{c_s^2\rho\,\delta_{ij} + \rho u_i u_j - P_{ij}\} = \frac{s_2}{2c_s^2\rho} Q_{ij} \tag{17}$$

where Q_{ij} are the terms in $\{\}$. Krafczyk et al. (2003) assumed that the Q_{ij}'s are functions of the non-equilibrium part of the DFs, $f_\alpha^{neq} = f_\alpha - f_\alpha^{eq}$ and provided their expressions as a function of the 2nd-order MRT moments. Similar to LES Eq. (10), they then calculated the turbulent viscosity as,

$$\nu_t = (C_S\Delta)^2|\mathbf{S}| = \frac{s_2}{2c_s^2\rho}(C_s\Delta)^2|\mathbf{Q}|, \qquad \text{with} \quad |\mathbf{Q}| = \sqrt{Q_{ij}Q_{ij}} \tag{18}$$

and expressed the relaxation rate of the 2nd-order moments as,

$$s_2 = \frac{1}{\tau_0 + \tau_t} \qquad \text{with} \quad \tau_t = \frac{1}{2}\left(\sqrt{\tau_0^2 + 18(C_s\Delta)^2|\mathbf{Q}|} - \tau_0\right) \tag{19}$$

where τ_0 is the relaxation time based on the molecular viscosity.

When applying the LES to the perturbation LBM, the moments P_{ij}^P are given by the last Eq. (14), yielding an expression for the perturbation rate of strain tensor that features nonlinear interaction terms between the I and P fields,

$$S_{ij}^P = \frac{s_2}{2c_s^2\rho}\left(c_s^2\rho\delta_{ij} + \rho_o u_i^P u_j^P + \rho_o u_i^I u_j^P + \rho_o u_i^P u_j^I - P_{ij}^P\right) = \frac{s_2}{2c_s^2\rho} Q_{ij}^P \tag{20}$$

The rate of strain tensor for the total flow is thus given by,

$$S_{ij} = \frac{s_2}{2c_s^2\rho} Q_{ij}^P + S_{ij}^I \tag{21}$$

Therefore the $|\mathbf{Q}|$ term to use in LES Eqs. (18) and (19) in combination with the MRT LBM Eqs. (11) to (15), is modified as follows,

$$|\mathbf{Q}| = \sqrt{R_{ij}R_{ij}} \qquad \text{with} \quad R_{ij} = Q_{ij}^P + \frac{2c_s^2\rho_o}{s_2} S_{ij}^I \tag{22}$$

where the Q_{ij}^P terms are computed with Eq. (20).

II – 4 LBM turbulent wall model

Typical naval hydrodynamics flows are fully turbulent, with $\mathrm{Re} > 10^6$. Thus, the turbulent boundary layers (BL) near solid boundaries (e.g., ship hull) must be properly modeled in the LBM. Since resolving the BL in the LBM grid would be computationally prohibitive

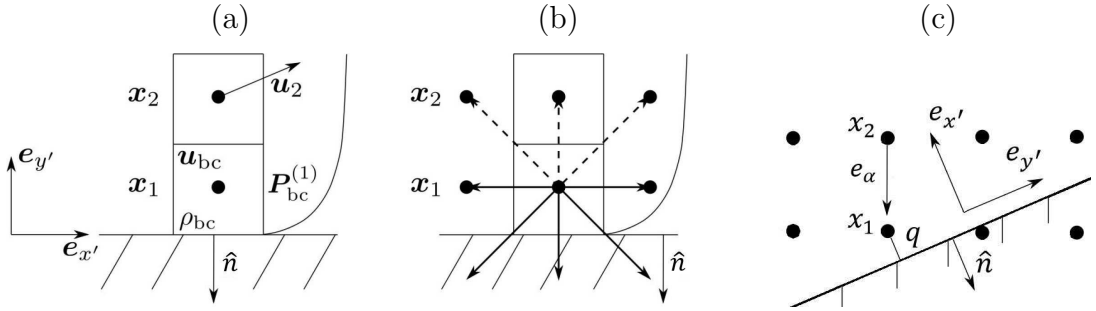

Figure 1 – Sketch of LBM flow reconstruction near a solid boundary (assumed 2D for simplicity) : (a) known or computed variables ; (b) known (——) and missing (- - - -) DF populations ; (c) variables in geometric calculations. Lattice points are marked by (•). [(a) and (b) from Malaspinas and Sagaut (2014)]

(even with grid refinement through nesting such as done in ELBE), besides the LES of the flow, this requires using a proper wall model. Below, we describe the extension to the perturbation LBM-LES of the method proposed by Malaspinas and Sagaut (2014), based on a macroscopic representation of the flow within the BL (i.e., on the LBM lattice). A thin layer approximation is introduced, implying that the mean free flow is locally nearly parallel to the solid boundary (i.e., wall) and statistically stationary ; it is also assumed that there is no horizontal pressure gradient. In such conditions, the mean velocity profile can be found as a function of the distance to the wall y from the semi-empirical equation proposed by Musker (1979), on the basis of experimentally validated logarithmic "laws of the wall" for the fully turbulent upper BL, the viscous lower BL, and a transition layer based on experimental measurements,

$$\tilde{u}(y^+) = u_\tau\left(\left(5.424\,\mathrm{atan}\left(\frac{2.0\,y^+ - 8.15}{16.7}\right) + \log_{10}\left(\frac{(y^+ + 10.6)^{9.6}}{(y^{+2} - 8.15\,y^+ + 86.0)^2}\right) - 3.52\right) \quad (23)$$

where the friction velocity u_τ and non-dimensional distance y^+ are defined as

$$u_\tau = \sqrt{\tau_w/\rho} \qquad \text{with} \quad y^+ = y\frac{u_\tau}{\nu} \quad (24)$$

Malaspinas and Sagaut (2014) also express the turbulent eddy viscosity as

$$\mu_t = \kappa y^+\left(1 - e^{\frac{-y^+}{26.0}}\right)^2\left|\frac{\partial\tilde{u}}{\partial y}\right| \quad (25)$$

and κ is a constant chosen to be 0.384 based on experimental data.

The "law of the wall" Eqs. (23) to (25) will be used to express the boundary condition at a solid boundary in the LBM, where unknown DF's are reconstructed on the lattice nodes based on the macroscopic flow quantities, assuming $\Delta x \gg \delta_{BL}$, with δ_{BL} the thickness of the viscous and transition sublayers in the BL. Let us define $\mathbf{x}_1$, $\mathbf{x}_2$, and $\hat{\mathbf{n}}$ as the position of the first and second off wall lattice nodes and the outward normal unit vector at the wall, respectively (Fig. 1). As is standard in most LBM wall boundary models, DF's that satisfy $\mathbf{e}_\alpha \cdot \hat{\mathbf{n}} < 0$ (dashed populations seen in Fig. 1b) are assumed to be unknown after the collision and propagation steps. To find the flow at $\mathbf{x}_1$ (labeled ρ_{bc} and $\mathbf{u}_{bc}$), these DFs are reconstructed using the velocity gradient at point 1 from the "law of the wall" combined with flow quantities calculated in the LBM at location $\mathbf{x}_2$. Thus, the DFs near the wall are constructed as,

$$f_\alpha(\mathbf{x}_1, t) = f^{eq}_\alpha(\rho_{bc}, \mathbf{u}_{bc}) + f^{neq}_\alpha\left(\frac{\partial\tilde{\mathbf{u}}_{bc}}{\partial y}\right) \quad (26)$$

where f_α^{eq} is specified through Equations (2) and (13) for the standard LBM or the perturbation LBM methods, respectively.

Details of determining flow quantities $\mathbf{u}_{bc}$ and ρ_{bc} at location $\mathbf{x}_1$ near the wall are discussed below. The f_α^{neq} DFs are constructed as follows (Malaspinas and Saugat 2014),

$$f_\alpha^{neq}\left(\frac{\partial \tilde{\mathbf{u}_{bc}}}{\partial y}\right) = -\frac{w_\alpha \rho}{c_s^2 \lambda_\nu} \sum_{i=1}^{3}\sum_{j=1}^{3}\{e_{\alpha i}e_{\alpha j} - c_s^2 I_{ij}\}S_{ij} \tag{27}$$

where λ_ν is the laminar relaxation time and I_{ij} is the identity matrix. While only validated in the present applications for a flat solid boundary (wall), this method is intended to be used for general boundary geometries, for which a shift in reference frame is needed, such that the x-axis always points towards the local streamwise direction. Here, the prime variables represent quantities shifted to a wall-normal reference frame (Fig. 1c), where location $\mathbf{x}_2$ is found by projecting $\hat{\mathbf{n}}$ along each lattice velocity at $\mathbf{x}_1$; we select the direction α with the largest y'_α value and find, $\mathbf{x}_2 = \mathbf{x}_1 + \mathbf{e}_\alpha \Delta t$. The streamwise basis vector $\mathbf{e}_{x'}$ is then computed by assuming that $\mathbf{x}_2$ lies within the BL. Thus,

$$y'_\alpha = \frac{\mathbf{e}_\alpha \cdot -\hat{\mathbf{n}}}{|\mathbf{e}_\alpha|}, \quad \text{with} \quad \mathbf{e}_{x'} = \frac{\mathbf{u}_2 - (\mathbf{u}_2 \cdot \hat{\mathbf{n}})\hat{\mathbf{n}})}{|\mathbf{u}_2 - (\mathbf{u}_2 \cdot \hat{\mathbf{n}})\hat{\mathbf{n}})|} \tag{28}$$

In many LBM solid boundary schemes, the distance between the wall and the nearest lattice point is assumed to be $\Delta x/2$. Here, a new scheme based on Merkle et al. (2016) is used to more accurately estimate this distance (see Fig. 1c). The calculation of y'_α and wall dependent quantities may then be more accurately performed within the wall model.

Specifically, to evaluate $\mathbf{u}'_{bc}$, which depends on the wall shear stress τ_w, for each near-wall lattice point, one numerically solves the implicit equation, $u'_2 = \tilde{u}(y'_2, \tau_w)$ where $\mathbf{u}'_2 = \mathbf{u}_2 \cdot \mathbf{e}'_x$ and $\tilde{u}(y'_2, \tau_w)$ is given by Musker's Eqs. (23) and (24). A Newton scheme is used to this effect, which iterates over the τ_w value until convergence. Next $\mathbf{u}_{bc}$ and μ_{bc} are solved for and Eq. (25) is used to specify the relaxation at boundary nodes, together with Eq. (19) and replacing the turbulent shear stress τ_t calculated with the LES by the newly calculated value τ_w. Finally, ρ_{bc} is calculated using the method originally proposed by Zou and He (1997), which reconstructs the flow density based on known DFs only,

$$\rho_{bc} = \frac{1}{1 + \tilde{\mathbf{u}}_{\mathbf{bc}} \cdot \hat{\mathbf{n}}}(2\rho_+ + \rho_0), \quad \text{with} \quad \rho_0 = \sum_{\alpha \in \alpha | \mathbf{e}_\alpha \cdot \hat{\mathbf{n}} = \mathbf{0}} f_\alpha \quad \text{and} \quad \rho_+ = \sum_{\alpha \in \alpha | \mathbf{e}_\alpha \cdot \hat{\mathbf{n}} > \mathbf{0}} f_\alpha \tag{29}$$

Equation (26) may now be applied to the unknown DFs (such as at point 2).

When applying this turbulent wall model to the perturbation LBM, we reconstruct the total flows, $\mathbf{u}_2$ and $\mathbf{u}'_2$ in Eq. (28) from $\mathbf{u}_2 = \mathbf{u}_2^I + \mathbf{u}_2^P$, and solve the macroscopic (Musker) equation to find $\mathbf{u}_{bc} = \mathbf{u}_1^I + \mathbf{u}_1^P$. The equilibrium DFs in Eq. (26) are now those of Eq. (13). Finally, in Eq. (27) we now use S_{ij}^P instead of S_{ij}, so that only the perturbation component is applied back to the DF's.

II – 5 Hybrid-LBM force evaluation

The total force acting on a solid body is computed in the perturbation LBM as a linear combination of the inviscid and perturbation forces, $\mathbf{F} = \mathbf{F}^I + \mathbf{F}^P$, where the inviscid contribution is evaluated through an integration over the body boundary Γ_B of the known pressure p^I. The perturbation force is evaluated through the momentum exchange method as,

$$\mathbf{F}^P = \sum_{\alpha \in \Gamma_B} \mathbf{F}_\alpha = -\frac{V}{\Delta t}\mathbf{e}_\alpha \{f_\alpha(t + \Delta t, \mathbf{x}) - f_{\alpha'}(t, \mathbf{x})\} \tag{30}$$

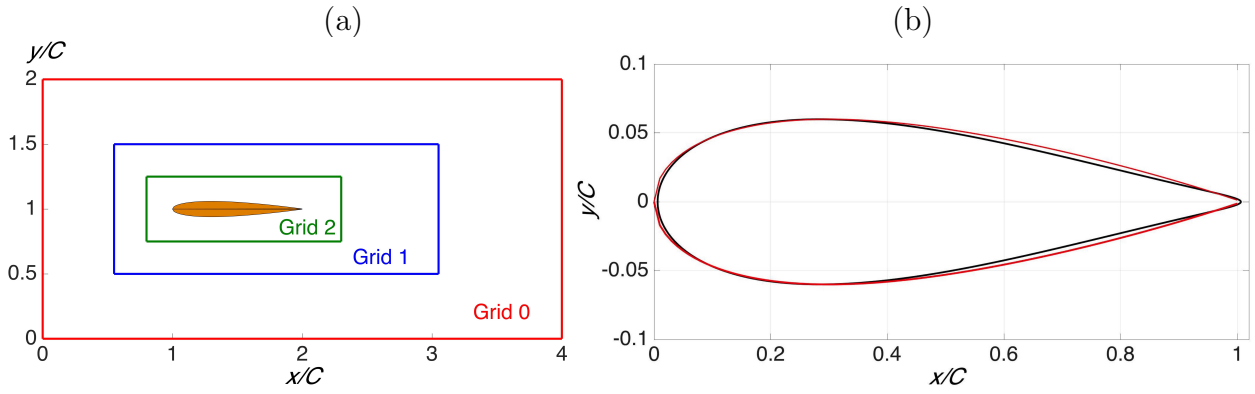

Figure 2 – Hybrid LBM-LES of flow past a NACA0012 hydrofoil of chord C : (a) nested LBM grid boundaries for large domain (Table 1). (b) cross-sections of a : (——) NACA0012 foil ; and (——) Karman-Trefftz foil used to compute the potential flow solution.

for all links α (with corresponding inverse direction α') that intersect the solid boundary, where V represents the grid cell volume. This equation expresses a difference in particle momentum before and after impacting the boundary and is a well established and accurate method for computing forces in the LBM, when the solid body is much larger than the grid spacing.

III – Applications

III – 1 Simulation of turbulent flow around a submerged hydrofoil

Here, we test the accuracy and efficiency of the perturbation LBM as compared to the standard LBM, both with LES but without a wall model, and particularly the accuracy of the force computations by the momentum exchange method. This is done by computing the turbulent flow around a NACA0012 foil (Fig. 2) as a function of its angle of attack θ, for a Reynolds number $\mathrm{Re} = UC/\nu = 3 \times 10^6$ (with U the free flow velocity, C the foil chord, and $\nu = 10^{-6}$ the water kinematic viscosity). We solve this as a 3D problem by placing the foil in a channel of length L, height H, and width W (Grid 0, Table 1). Because there is no wall model, we only consider results for the lift force on the foil, $F_L = (1/2)\rho C_L W C$, which is caused mainly by differences in pressure distribution rather than by shear at the solid boundary. It is anticipated that the addition of a turbulent wall model to this test case will further improve results.

In all cases we use nested LBM grids, increasingly resolved towards the foil : 3 for the standard LBM (Table 1 and Fig. 2a) and 2 for the perturbation LBM (Table 2 and Fig. 3a). Boundary conditions are specified as follows, for the standard or perturbation LBMs, respectively : (i) periodic conditions on sidewall boundaries ($z = 0$ and W) ; (ii) a specified velocity $\mathbf{u} = U\mathbf{e}_x$ or a gradient free condition, on the inlet ($x = 0$) and upper/bottom boundaries ($y = 0$ and H) ; (iii) a specified velocity $\mathbf{u} = 0$ or $\mathbf{u}^P = -\mathbf{u}^I$, on the foil boundary Γ_B ; and (iv) a gradient free condition on the outlet boundary ($x = L$; i.e., no change in $\mathbf{u}$ downstream). In the LBM, periodicity is achieved by specifying periodic DFs, velocity is prescribed on a boundary by specifying the DFs, and a gradient free condition reads, $\partial \mathrm{DFs}/\partial\tilde{n} = 0$ (i.e., $\nabla f_\alpha \cdot \tilde{\mathbf{n}} = 0$ or $\nabla f_\alpha^P \cdot \tilde{\mathbf{n}} = 0$). More specifically, in the perturbation LBM, condition (iii) on the foil boundary is implemented via a standard "bounce forward"

Grid Number	L/C	W/C	H/C	$\Delta x/C$	N
Grid 0	4.0	2.0	0.2	0.0182	293,040
Grid 1	2.5	1.5	0.15	0.0913	556,416
Grid 2	1.5	0.5	0.5	0.0045	892,416

TABLE 1 – Grid parameters of the large domain used in the initial tests of the regular and hybrid LBM-LES models, for the submerged hydrofoil test case (Figs. 3 and 5). Grid length is L, width W, height H, and hydrofoil chord length C. Total number of LBM points is $N = 1,741,872$.

Grid Number	L/C	W/C	H/C	$\Delta x/C$	N
Grid 0	2.9	1.2	0.2	0.0081	1,404,000
Grid 1	2.0	0.8	0.15	0.0040	3,984,000

TABLE 2 – Grid parameters of small domain used in convergence tests of the perturbation LBM-LES model for the submerged hydrofoil test case (Figs. 4 and 5). Grid length is L, width W, height H, and hydrofoil chord length C. Total number of LBM points is $N = 5,388,000$.

scheme applied to the DFs after the collision and propagation steps,

$$f_{\alpha'}(\mathbf{x}_1, t) = f_\alpha(\mathbf{x}_1, t) - 2\rho_0 w_\alpha \frac{\mathbf{e}_\alpha \cdot -\mathbf{u}^I}{c^2} \tag{31}$$

where direction α' is opposite to direction α; Eq. (31) is applied to all boundary nodes that satisfy the condition $\mathbf{e}_{\alpha'} \cdot \tilde{\mathbf{n}} < 0$.

The inviscid fields ($\mathbf{u}^I$, p^I) are analytically calculated at each LBM node based on a conformal mapping solution for a Karman-Trefftz foil that is very similar in shape to the NACA0012 foil (Fig. 2b). In future more complex cases this solution will be computed with an inviscid BEM model (see Harris et al. in this conference). Using the discretizations of Tables 1 and 2, both the LBM and perturbation LBM methods need approximately 10 minutes on the GPGPU to simulate four seconds of steady state, for a given angle of attack. An example of flow velocity obtained for a stalling case with the perturbation LBM is shown in Fig. 3b. For both LBM methods, convergence of the lift coefficient C_L was assessed for incidence angles $\theta = 0$ to 10 deg. Fig. 4 shows the C_L values computed as a function of θ with various methods, as compared to laboratory experiments in a wind tunnel (Abbot and Doenhoff 1959). A good

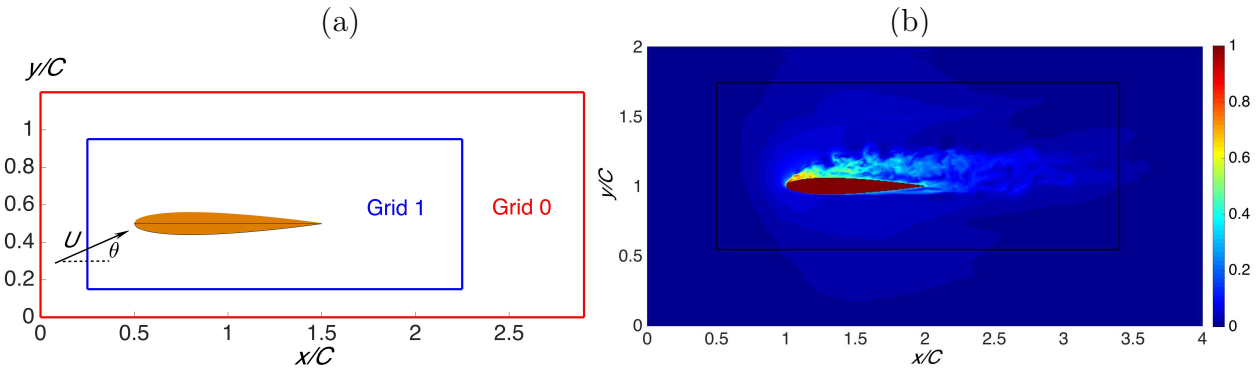

Figure 3 – Perturbation LBM-LES of flow past a NACA0012 hydrofoil of chord C : (a) nested LBM grid boundaries for small domain (Table 2); (b) normalized perturbation velocity magnitude $|\mathbf{u}|/U$ for a stalling foil at $\theta = 14$ deg. The black box represents the outer extent of the domain used in the hybrid LBM convergence tests.

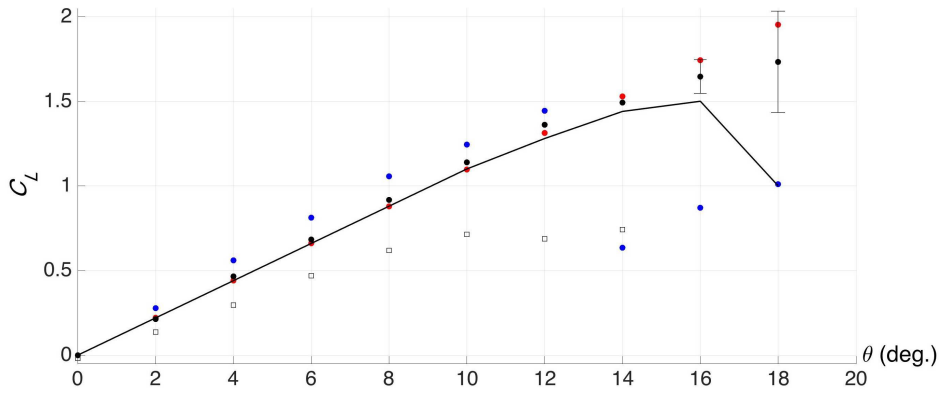

Figure 4 – Lift coefficient C_L of a NACA0012 foil as a function of its angle of attack θ for Re $= UC/\nu = 3 \times 10^6$ (U is flow velocity, C is chord length, and ν the fluid kinematic velocity), in (——) wind tunnel experiments (Abbot and Doenhoff, 1959) and computations with a : (•) Potential flow method ; (□) LBM ; (•) perturbation LBM (larger original domain ; Fig. 2) ; (•) perturbation LBM (reduced domain size ; Fig. 3). The brackets at high θ values reflect oscillations in the computed lift force due to stalling.

agreement is observed for the potential flow solution at low angles of attack $\theta \leq 12$ deg. ; this is expected in this high Re number regime. However at larger angles of attack, flow separation starts occurring with increased viscous/turbulent effects and the inviscid solution overpredicts lift and misses stall. The standard LBM solution does not predict C_L very well, likely because the grid is too coarse in this large domain and numerical dissipation is caused by the foil boundary condition. The y^+ values are on the order of 100 at the first fluid cells nearest the foil boundary, which leads to underpredicting flow momentum near the foil, causing early separation and reduced lift. Future work will involve adding the turbulent wall model detailed above to the LBM, for solid boundaries of arbitrary geometry, and it is anticipated that this will produce a significant improvement in lift and stall prediction, as well as provide an accurate drag estimate. The perturbation LBM predicts C_L much better, even when applied to the larger and coarser original domain (with $N \simeq 1.7 \times 10^6$), but more so when applied to the smaller higher resolution domain (with $N \simeq 5.4 \times 10^6$). This confirms the advantage of forcing the LBM with the inviscid flow, which allows for a more accurate computation of the total flow with the LBM. For this test case, at low angles of attack, there should be a very small lift force provided by the perturbation flow but this requires using a sufficiently refined LBM discretization to be captured. Stall is observed to start occurring for $\theta \geq 12$ degrees, leading to increased oscillations in the computed lift force, as θ increases ; this is consistent with the physics of the problem as vortex shedding starts occurring (Fig. 3b). Complete stall occurs at approximately 16 degrees, when large oscillations in lift force are observed and the average C_L value starts decreasing (denoted by the brackets in Fig, 4). The earlier stall observed in the perturbation LBM results is likely caused by inaccuracies near the foil boundaries present in the LBM from the lack of a wall model ; this will be addressed in future work.

By nature, the perturbation LBM domain should only extend away from the foil in the region where viscous effects are important. Hence, for many test cases (such as streamlined bodies), the perturbation LBM domain can be much smaller than the domain required to accurately compute the inviscid flow, allowing for a significant increase in computational efficiency. This was confirmed when using the reduced domain of Figure 3a (Table 2), which led to much more accurate C_L values. The extent of the different domains were chosen through a visual inspection of stalling in standard LBM results. Furthermore the overall

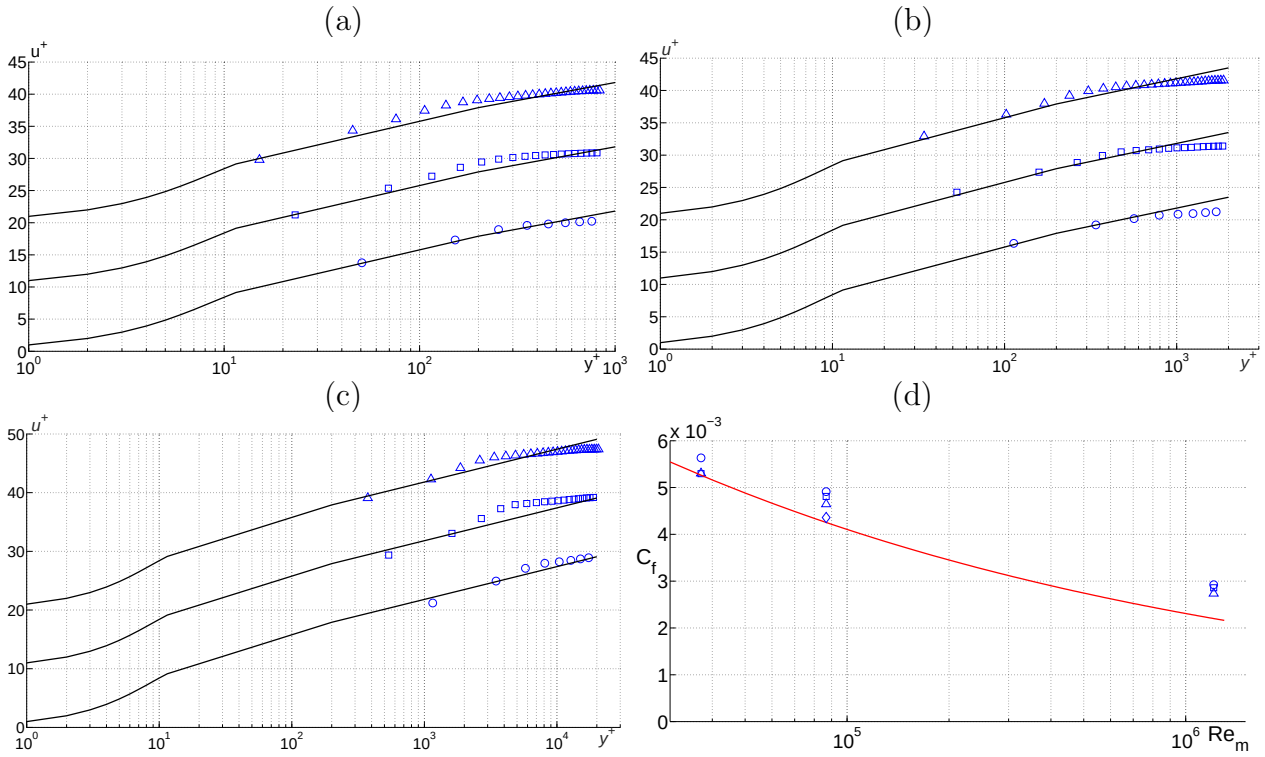

Figure 5 – Simulation of turbulent flow past a flat plate with the perturbation LBM. (a-c) Mean velocity u^+ as a function of distance y^+ above the plate, at Re_m = (a) 37,042, (b) 86,773, and (c) 1.21×10^6. Numerical results (symbols) are plotted for a half channel of resolution N = (○) 10, (□) 20, and (△) 30, compared to Musker's (1979) velocity profile (——). For visualization purposes, for $N = 20$ and 30, the latter are shifted by $\Delta u^+ = 10$ and 20, respectively. (d) Bulk friction coefficient C_f computed as a function of the mean Reynolds number Re_m (besides earlier values, one additional result is shown at $N = 40$ (◇) for $Re_m = 86,773$), compared to Dean's (1976) correlation for turbulent channels (——).

discretization of the reduced domain was increased, with the intent to improve convergence.

III – 2 Simulation of turbulent flow over a flat plate

Here, we validate the turbulent wall model in the context of the perturbation LBM by simulating a turbulent flow over a flat plate; results are compared to those of the standard LBM. Similar to Malaspinas and Sagaut's (2014) test case, we use a parallelepipedic domain of dimensions, $L = 2\pi M$, $H = 2M$, and $W = 2\pi M$ (M denoting the half channel width), with flat plates specified on the lower/upper boundaries at $y = 0$ and H, on which the turbulent wall model is applied, and periodic boundary conditions in the 2 horizontal directions at $x = 0$ and L (streamwise) and $z = 0$ and W (cross stream).

In this application, the flow is forced by way of a body force (term B'_α in LBM Eq. (2); see, Cabrit, 2009), $F = \{u_\tau^2 + u_m(u_m - u_x)\}/M$, in which u_x is the instantaneous space-averaged downstream velocity component. The inviscid velocity field specified in the perturbation LBM is uniform over the channel, $\mathbf{u}^I = U\mathbf{e}_x$, where U is calculated by applying the law of the wall Eq. (23) at the center of the channel, i.e., $\tilde{u}(y^+)$ for $y = H/2$. The Smagorinsky constant used in the LES is set to $C_S = 0.16$ in all simulations, which is in the middle of the range of recommended values. Each simulation is run until both a fully turbulent flow is observed and a quasi-steady mean flow is achieved.

We tested flows for 3 values of the Reynolds number, $\mathrm{Re}_\tau = Mu_\tau/\nu$ = 950, 2,000, and

20,000 based on the friction velocity u_τ, or $\mathrm{Re}_m = 2Mu_m/\nu = 37,042$, 86,773, and 1.21×10^6 based on the average bulk velocity u_m in the x direction, obtained from Dean's (1976) correlation. Each case was simulated in 3 LBM discretizations, for which $\Delta x = \Delta y = \Delta z = M/N$, with $N = 10$, 20, and 30; in the middle Re case, we also tested $N = 40$. The full channel width is thus discretized with $2N$ LBM points in the y direction.

Figures 5a,b,c show the velocity profiles computed for each simulated Re value with the perturbation LBM-LES; almost identical results were obtained using the standard LBM-LES, which further confirms the relevance and accuracy of the decomposition method. In all cases, results agree well with Musker's (1979) profile for the smaller $y+$ values. At higher y^+ values, however, velocities are slightly underperdicted in the LBM, which is likely the result of having 2 plates in the model, with a finite separation distance H, rather than a free flow past a single plate, which is the case of Musker (1979). Using the law of the wall to specify the boundary condition just above the solid boundary, we see that the LBM-LES is able to accurately capture the velocity profile in the intermediate and turbulent BLs, without need for a fine discretization and in particular for resolving the viscous BL. For the largest Re, the method is pushed to its limits, with the resolution being such that $y_1^+ = 333$, 500, and 1000 at the first LBM point ($\mathbf{x}_1$ in Fig. 1), for the different N values, which is quite large; the latter is a very under-resolved test, but one that demonstrates the overall robustness of the method.

As the LBM grid resolution increases, for all Re_τ or Re_m values, velocity profiles agree better with Musker's profile and, hence, one would expect that the shear stress and friction coefficient computed on the plate would also become more accurate. This is verified in Fig. 5d which compares, for the 3 Re values, the computed bulk friction coefficient $C_f = 2u_\tau^2/u_m^2$, to Dean's (1976) correlation, which is based on experiments. For the lowest Re value, $Re_m = 37,042$, convergence to the reference solution with increasing N is achieved, indicating that the BL is adequately resolved for $N = 20$ or 30, for which the first lattice point ($\mathbf{x}_1$) corresponds to $y_1^+ = 24$ or 16 in Fig. 5a. A convergence trend is also seen for the higher Re values, but convergence is not achieved; for $Re_m = 86,773$, the simulation was run for an additional finer resolution with $N = 40$, corresponding to $y_1^+ = 25$, for which convergence to the reference solution was nearly achieved. Results thus indicate that $y_1^+ \simeq 25$ is the coarser discretization to achieve accurate shear and drag computations in the LBM. Finally, there is again negligible differences between C_f values calculated with the standard LBM or the perturbation LBM.

IV – Conclusions

We presented a new hybrid model combining potential flow and NS-LBM-LES solvers, for naval hydrodynamics problems. Simple applications for a submerged foil and a turbulent channel demonstrated both the relevance and accuracy of the hybrid approach, as well as a close agreement between results of the standard and perturbation LBM-LES models. It should be pointed out, however, that the inviscid rate of strain tensor was zero in the turbulent channel, but present for the turbulent hydrofoil simulations; hence a more rigorous validation will be done in future work. Additionally, future work will consider drag computation using the wall model for more complex geometries such as the hydrofoil. Drag on such bodies is much smaller than lift and hence its accurate computation is more challenging, particularly for high Re values.

The main advantage of the perturbation LBM, its ability to use a smaller domain to solve the NS equations relative to standard solvers, hence allowing both higher resolution and efficiency, has not yet been fully explored and will also be the object of future work in

which the far-field inviscid flow is more complex (e.g., irregular wave field). Finally, earlier work by O'Reilly et al. (2015) has illustrated the standard LBM model's (ELBE) ability to also simulate free surface flows and free surface piercing bodies. We intend to extend the perturbation LBM method to simulating such problems, using fully non-linear free surface boundary conditions in which "I-P" interaction terms will appear.

V – Acknowledgements

C. O'Reilly, S. Grilli, A. Mivehchi and J. Dahl acknowledge support from grants N000141310687 and N000141612970 of the Office of Naval Research (PM Kelly Cooper).

References

[1] Abbot, I.H., Von Doenhoff A.E. (1959) *Theory of Wing Sections*, Dover Pub., New York.

[2] Alessandrini, B. (2007). *Thèse d'Habilitation en Vue de Diriger les Recherches*. Ecole Centrale de Nantes, Nantes.

[3] Banari A., Janssen C.F., and Grilli S.T. (2014). An efficient lattice Boltzmann multiphase model for 3D flows with large density ratios at high Reynolds numbers. *Comp. and Math. with Applications*, **68**(12), 1819-1843.

[4] Cabrit, O. (2009) Direct simulations for wall modeling of multicomponent reacting compressible turbulent flows. *Phys. Fluids*, **21**, 055108.

[5] Dean, R. B., (1976) A single formula for the complete velocity profile in a turbulent boundary layer. *J. Fluids Eng.*, **98**(4), 723-726.

[6] Grilli, S.T. (2008) On the Development and Application of Hybrid Numerical Models in Nonlinear Free Surface Hydrodynamics. Keynote lecture in *Proc. 8th Intl. Conf. on Hydrodynamics* (Nantes, France, 9/08) (P. Ferrant and X.B. Chen, eds.), pps. 21-50.

[7] Grilli, S.T., Dias, F., Guyenne, P., Fochesato, C. and F. Enet (2010) Progress In Fully Nonlinear Potential Flow Modeling Of 3D Extreme Ocean Waves. Chapter 3 in *Advances in Numerical Simulation of Nonlinear Water Waves* (ISBN : 978-981-283-649-6, edited by Q.W. Ma) (Vol. 11 in Series in Advances in Coastal and Ocean Engineering). World Scientific Publishing Co. Pte. Ltd., pps. 75- 128.

[8] Guo Z., Zheng C., and Shi B. (2002). Discrete lattice effects on the forcing term in the lattice Boltzmann method. *Phys. Rev.*, **E65**(4).

[9] Harris, J.C. and S.T. Grilli (2012). A perturbation approach to large-eddy simulation of wave-induced bottom boundary layer flows. *Intl. J. Numer. Meth. Fluids*, **68**, 1,574-1,604.

[10] Harris J.C. and Grilli, S.T. (2014). Large eddy simulation of sediment transport over rippled beds. *Nonlin. Process. Geophys.*, **21**, 1,169-1,184.

[11] d'Humieres D., Ginzburg I., Krafczyk M., Lallemand P., and Luo L.-S. (2002) Multiple Relaxation-Time Lattice Boltzmann models in three-dimensions. *Phil. Trans. Royal Soc. London*, **A360**, 437-451.

[12] Janssen C.F., S.T. Grilli and M. Krafczyk (2010) Modeling of Wave Breaking and Wave-Structure Interactions by Coupling of Fully Nonlinear Potential Flow and Lattice-Boltzmann Models. In *Proc. 20th Offshore and Polar Engng. Conf.* (ISOPE10, Beijing, China, June 20-25, 2010), pps. 686-693. Intl. Society of Offshore and Polar Engng.

[13] Janssen, C.F. (2010) *Kinetic approaches for the simulation of non-linear free surface flow problems in civil and environmental engng.*. PhD thesis, Technical Univ. Braunschweig.

[14] Janssen, C.F., S.T. Grilli and M. Krafczyk (2013) On enhanced non-linear free surface flow simulations with a hybrid LBM-VOF approach. *Comp. and Math. with Applications*, **65**(2), 211-229.

[15] Janssen, C.F., D. Mierke, M Überrück, S. Gralher, and T. Rung (2015) Validation of the GPU-accelerated CFD solver ELBE for free surface flow problems in civil and environmental engineering. *Computation*, **3**(3),354-385.

[16] Janssen, C.F., Rung, T., Grilli S.T., O'Reilly C.M., (2016) An enhanced LBM-based perturbation method (in preparation).

[17] Krafczyk M., Tölke J., Rank E., and Schulz M. (2001) Two-dimensional simulation of fluid-structure interaction using Lattice Boltzmann methods. *Comp. and Struct.*, **22**, 2,031-2,037.

[18] Krafczyk M., Tölke J., and Luo L.-S. (2003) Large eddy simulations with a multiple-relaxation-time LBE model. *Intl. J. Modern Phys.*, **17**, 33-39.

[19] Lallemand, P. and Luo, L.S. (2000) Theory of the Lattice Boltzmann Method : Dispersion, dissipation, isotropy, Galilean invariance, and stability. *Phys. Review*, **E61**, 6,546-6,562.

[20] Malaspinas, O., Sagaut, P., (2014) Wall model for large-eddy simulation based on the lattice Boltzmann method. *J. Comp. Phys.*, **257**, 25-40.

[21] Merkle, D., Janssen, C.F., (2016) Efficient calculation of sub-grid distances for higher-order boundary conditions in LBM (in preparation).

[22] Musker, A. (1979) Explicit expression for the smooth wall velocity distribution in a turbulent boundary layer. *AIAA J.*, **17**(6), 655-657.

[23] O'Reilly, C., Grilli, S.T., Dahl, J.M., Banari, A., Janssen, C.F., Shock, J.J. and M. Uberrueck. (2015) Solution of viscous flows in a hybrid naval hydrodynamic scheme based on an efficient Lattice Boltzmann Method. In *Proc. 13th Intl. Conf. on Fast Sea Transportation* (FAST 2015 ; Washington D.C., September 1-4, 2015).

[24] Reliquet, G., A. Drouet, P.-E. Guillerm, L. Gentaz and P. Ferrant (2014). Simulation of wave-ship interaction in regular and irregular seas under viscous flow theory using the SWENSE method. In *Proc. 30th Symp. Naval Hydrod.* (Tasmania, 11/2014), 11 pps.

[25] Succi, S. (2002) *The lattice Boltzmann equation for fluid dynamics and beyond*, Oxford Science Publications, Oxford.

[26] Zou Q., He X. (1997) On pressure and velocity boundary conditions for the lattice Boltzmann BGK model, *Phys. Fluids*, **9**, 1,592-1,598.